Tuning the Magic Size of Atomically Precise Gold Nanoclusters via Isomeric Methylbenzenethiols

4 AUTHORS, INCLUDING:

Yuxiang Chen
Carnegie Mellon University
14 PUBLICATIONS   **100** CITATIONS

SEE PROFILE

Chenjie Zeng
Carnegie Mellon University
27 PUBLICATIONS   **598** CITATIONS

SEE PROFILE

Tuning the Magic Size of Atomically Precise Gold Nanoclusters via Isomeric Methylbenzenethiols

Yuxiang Chen,[†] Chenjie Zeng,[†] Douglas R. Kauffman,[‡] and Rongchao Jin*,[†]

[†]Department of Chemistry, Carnegie Mellon University, Pittsburgh, Pennsylvania 15213, United States
[‡]National Energy Technology Laboratory (NETL), United States Department of Energy, Pittsburgh, Pennsylvania 15236, United States

S *Supporting Information*

ABSTRACT: Toward controlling the magic sizes of atomically precise gold nanoclusters, herein we have devised a new strategy by exploring the para-, meta-, ortho-methylbenzenethiol (MBT) for successful preparation of pure $Au_{130}(p\text{-}MBT)_{50}$, $Au_{104}(m\text{-}MBT)_{41}$ and $Au_{40}(o\text{-}MBT)_{24}$ nanoclusters. The decreasing size sequence is in line with the increasing hindrance of the methyl group to the interfacial Au−S bond. That the subtle change of ligand structure can result in drastically different magic sizes under otherwise similar reaction conditions is indeed for the first time observed in the synthesis of thiolate-protected gold nanoclusters. These nanoclusters are highly stable as they are synthesized under harsh size-focusing conditions at 80−90 °C in the presence of excess thiol and air (i.e., without exclusion of oxygen).

Subtle Change of Protecting Thiolate Ligands

$Au_{130}(p\text{-}MBT)_{50}$ $Au_{104}(m\text{-}MBT)_{41}$ $Au_{40}(o\text{-}MBT)_{24}$

Drastically Different Magic Sizes for Gold Nanoclusters

**KEYWORDS:** *Gold, nanocluster, atomic precision, tunable magic sizes, isomeric methylbenzenethiols, Au−S bond*
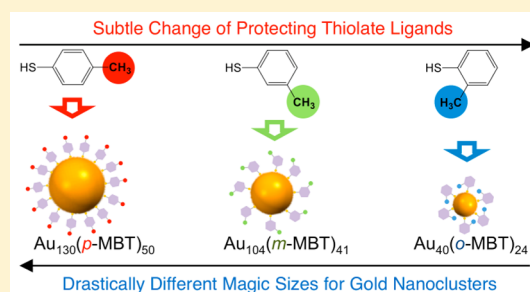
tomically precise gold nanoclusters protected by ligands have emerged as a new class of nanomaterials,[1−12] which hold potential in a wide range of applications including catalysis, optics, energy, and biomedicine owing to their unique physical and chemical properties.[13−22] To uncover the fundamental aspects of atomically precise gold nanoclusters and develop new applications, it is of critical importance to devise synthetic strategies for obtaining different magic sizes of nanoclusters with true monodispersity.[23−27] It has been established that magic-sized gold nanoclusters possess superior stabilities and can thus be obtained via selective growth under harsh conditions such as high temperature and the presence of excess thiol and oxygen, under which those less stable sizes are converted to stable ones or decomposed and eventually a single size is attained.[25,28,29]

Recently, the surface-protecting thiolates were found to be capable of affecting the magic sizes and structures of gold nanoclusters.[30−34] For example, Tsukuda and co-workers showed that if an extremely bulky thiolate was applied, new gold−thiolate surface protecting motifs might emerge, which gave rise to a new $Au_n(SR)_m$ size.[31] We demonstrated that the existing magic-sized gold nanoclusters can be transformed into new ones through ligand exchange with a distinctly different thiol, and a notable example is the transformation of the biicosahedral $Au_{38}(SC_2H_4Ph)_{24}$ nanocluster to tetrahedral $Au_{36}(TBBT)_{24}$ (TBBT = $SPh\text{-}p\text{-}{}^{t}Bu$).[32,33] On the other hand, it was also found that some nanoclusters (e.g., $Au_{25}(SR)_{18}$) are compatible with a wide range of ligands of various bulkiness (such as glutathione, SC_nH_{2n+1}, SC_2H_4Ph, etc.) under different synthetic conditions.[35−37] Thus, it is still unclear how sensitive

the nanocluster synthesis is to the ligand structure and whether the thiolate ligand effect can be utilized for systematic size control remains to be explored. The intriguing role of some special thiolate ligands motivates us to devise a new synthetic route for size-controlled synthesis of different magic-sized gold nanoclusters based on the ligand selection.

Herein, we report a surprising finding that under similar synthetic conditions, a subtle change of the thiolate ligand structure, demonstrated with three isomeric methylbenzenethiols ($p/m/o$-MBT, Scheme 1) can have significant effects on the resulting size of gold nanoclusters. Our results show that different magic sizes of gold nanoclusters (Au_{130}, Au_{104}, and Au_{40}) are thermodynamically selected by p-MBT, m-MBT and o-MBT, respectively, under the size-focusing conditions. This

Scheme 1. Molecular Structures of the Three Isomeric Methylbenzenethiols. Color Codes: Yellow, Sulfur; Grey, Carbon; White, Hydrogen

p-MBT m-MBT o-MBT
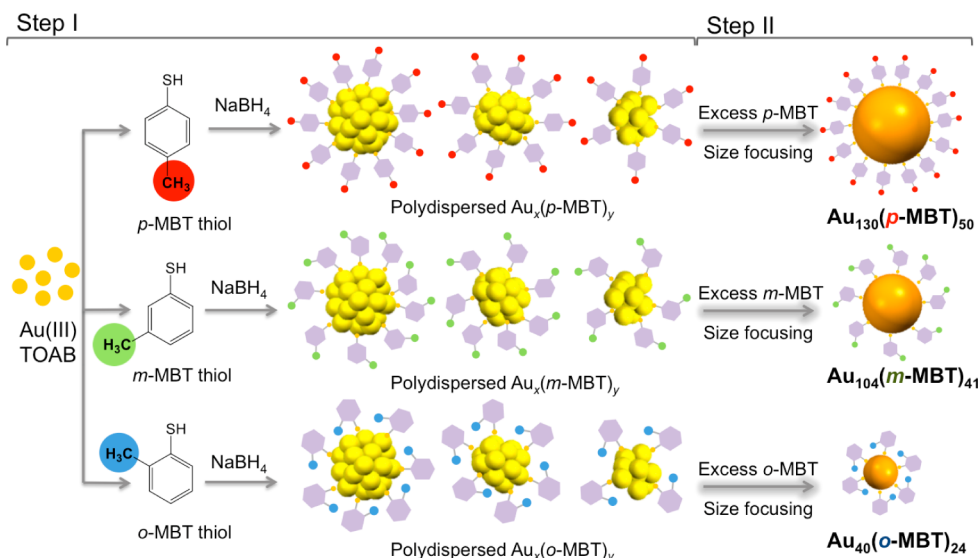
Subtle change of ligand structure
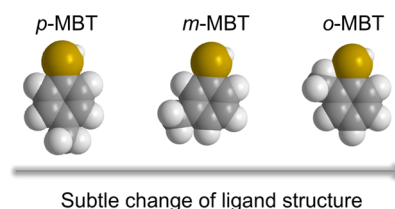
Figure 1. Two-step size-focusing syntheses of different magic-sized nanoclusters by exploring the three isomeric thiol ligands: p-MBT, m-MBT, and o-MBT.

magic-size tunability with the three isomeric thiols is remarkable, considering their only difference being the methyl group's position in the ligand. Interestingly, when the methyl group on the benzene ring changes from para to meta then to ortho position, a clear trend of decreasing size from Au_{130} to Au_{104} to Au_{40} has been observed. This discovery provides new insights into the unexpected role of structurally similar thiols in the size-controlled synthesis of atomically precise gold nanoclusters and also reveals some insights into how the thiolate ligands dictate the magic sizes and determine their stability. This method of Au−S interfacial bond engineering adds a new dimension to the ligand-based strategy for controlled synthesis of nanoclusters.

The detailed synthetic strategy is illustrated in Figure 1. We explored the p-MBT, m-MBT, and o-MBT ligands for size-controlled syntheses of gold nanoclusters via two steps (see the Supporting Information for details). In step I, a size-mixed nanocluster crude product protected by p-MBT, m-MBT, or o-MBT thiol, respectively, was first prepared. Briefly, gold salt ($HAuCl_4$, 0.4 mmol) was phase transferred from an aqueous solution to toluene with the aid of tetraoctylammoniun bromide (TOAB, 0.46 mmol), and then Au(III) was reduced to Au(I) by adding thiol (2 mmol), and eventually Au(I)SR was reduced to Au(0) nanoclusters by $NaBH_4$ (4 mmol). In step II, the polydispersed crude product obtained from step I was subject to size-focusing through etching with excess thiols at elevated temperatures. The final products were obtained and the formulas were determined to be $Au_{130}(p$-MBT$)_{50}$, $Au_{104}(m$-MBT$)_{41}$, and $Au_{40}(o$-MBT$)_{24}$, respectively (Figure 1).

We first discuss the case of p-MBT. The essence of the size-focusing methodology is to transform the initially polydispersed gold nanoclusters into monodispersed magic size nanoclusters under harsh conditions, resulting in "survival of the most robust".[28] Matrix-assisted laser desorption ionization (MALDI) mass spectrometry was applied to characterize both the pre- and postfocusing nanoclusters. For the crude product from step I, MALDI analysis showed a distribution of sizes for p-MBT protected gold nanoclusters (Figure 2a, black profile). In step II, the size distribution was narrowed down and eventually focused into one single species with mass around 31 kDa,

labeled as M_p (Figure 2a, red profile). Of note, the tiny peak at m/z = 15.5 k (z = 2) was the doubly charged peak of the M_p species. The optical absorption spectrum of the M_p nanoclusters showed prominent bands at ∼390, ∼490, ∼605, and ∼700 nm (Figure 2b). The steplike spectrum is typical of quantum-sized gold nanoclusters (core size <2 nm) due to multiple one-electron transitions, as opposed to the plasmon resonance for gold nanoparticles in the 2−100 nm size regime. It is also worth noting that such distinct molecular-like optical features of gold nanoclusters often indicate monodispersity, as size-mixed nanoclusters readily wash out such features and give rise to a featureless, decay-like spectrum.[23]

In order to obtain the precise formula of this M_p species, we further performed electrospray ionization (ESI) mass spectrometry to determine the exact molecular weight of the MALDI-determined 31 kDa species. In ESI analysis, CsOAc was added to produce positively charged adducts in the ESI process. Two intense peaks were observed at m/z = 10721.09 and 16015.04 (Figure 2c and Supporting Information Figure S1a,b), which are assigned to the triply charged $[M_pCs_3]^{3+}$ and doubly charged $[M_pCs_2]^{2+}$, respectively. Thus, the molecular weight of the M_p species is determined to be 31764.54 based on the 3+ peak (i.e., 10721.09 × 3−132.91 × 3), and 31764.26 based on the 2+ peak (i.e., 16015.04 × 2−132.91 × 2). The average molecular weight of M_p nanoclusters is thus 31764.40, which is consistent with the MALDI-determined 31 kDa (albeit some ligands were lost due to laser irradiation in MALDI analysis). We also performed thermogravimetric analysis (TGA) to determine the Au/SR molar ratio. In the TGA profile, a weight loss of 19.6% was observed (Figure 2d), corresponding to a Au/SR molar ratio of 1/0.39. Of note, thermal decomposition of $Au_n(SR)_m$ in the TGA analysis gives rise to yellow gold and gaseous RS-SR disulfide; no sulfur atoms were left in the resultant yellow gold. On the basis of the determined molecular weight (31764.40) and Au/S ratio (1/0.39), we deduced the exact formula of the M_p nanocluster by screening a series of possible numbers of gold atoms and thiolate ligands (Supporting Information Table S1). Only the $Au_{130}(p$-MBT$)_{50}$ formula is in agreement with both the experimental molecular weight (theoretical, 31765.12; deviation
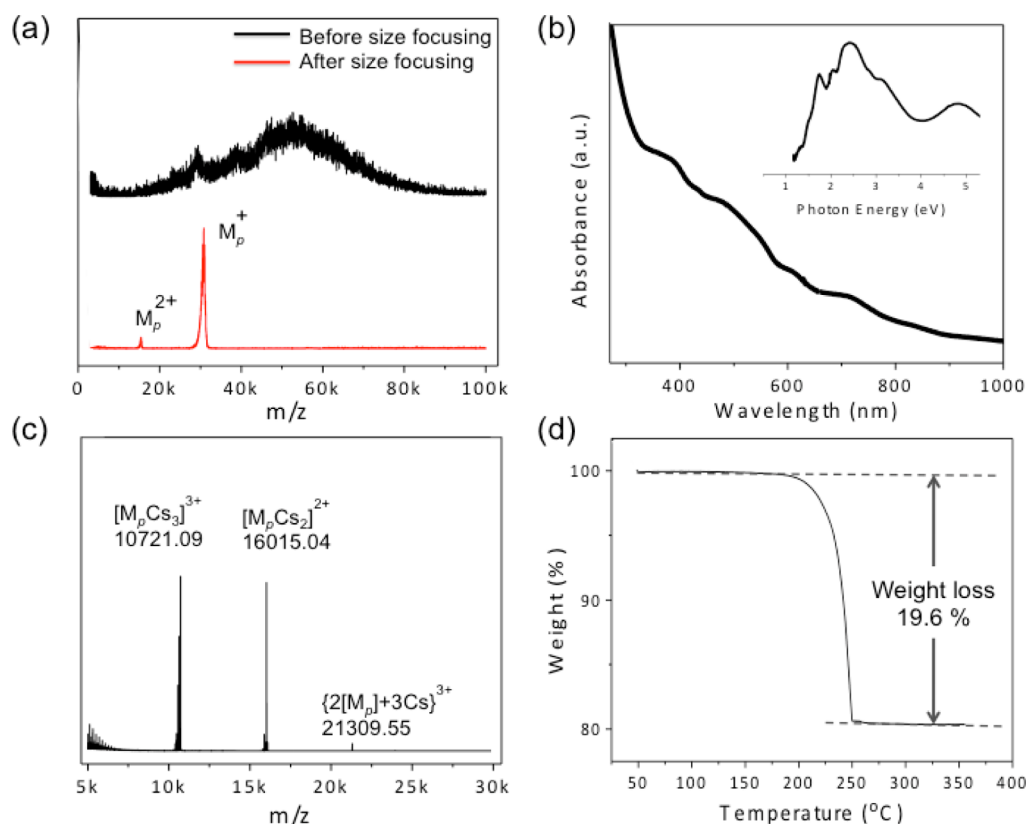
Figure 2. $Au_{130}(p\text{-MBT})_{50}$ nanocluster. (a) MALDI-MS of the nanocluster before/after size-focusing; (b) UV−vis spectrum, inset: photon-energy plot; (c) ESI-MS; (d) TGA.

0.72) and the TGA weight loss (theoretical, 19.4%; deviation −0.2%). Thus, the 31 kDa species is unequivocally determined to be $Au_{130}(p\text{-MBT})_{50}$, and accordingly the small peak at m/z = 21309.55 in the ESI-MS (Figure 2c) is due to the formation of $\{2[Au_{130}(p\text{-MBT})_{50}]+3Cs\}^{3+}$ (theoretical, 21309.84; deviation 0.29), which further confirms the cluster formula.

It is worth noting that if 2-phenylethylthiol (PhC_2H_4SH) or long-chain aliphatic thiol ($C_nH_{2n+1}SH$) was used in this two-step size-focusing method under similar synthetic conditions, the ubiquitous $Au_{144}(SR)_{60}$ ($SR = SC_2H_4Ph$ or SC_nH_{2n+1}) nanoclusters were produced as the final products.[38,39] Negishi et al. previously reported that $Au_{130}(SC_{12}H_{25})_{50}$ can be separated from $Au_{144}(SC_{12}H_{25})_{60}$ and other sizes by tuning $[AuCl_4^-]/[HSR]$ ($SR = SC_{12}H_{25}$) to 1:1.[40] Interestingly, in our present study by choosing p-MBT as the protecting thiol there is no $Au_{144}(p\text{-MBT})_{60}$ present in the final product, which gives us an important implication that thiolate ligands may play an important role in tuning and selecting the magic sizes under the size focusing conditions. This is also significant in the sense of synthesizing pure gold nanoclusters; by changing the thiolate ligand, the $Au_{130}(SR)_{50}$ magic size which was difficult to synthesize in pure form previously (i.e., without nontrivial separation) can now be obtained readily. In Supporting Information Figure S2, the optical spectra of relevant $Au_{130}(SR)_{50}$ nanoclusters reported previously[40−42] are compared with the present $Au_{130}(p\text{-MBT})_{50}$ nanocluster (Supporting Information Figure S2, panel A); the latter shows fine features, indicating very high purity, as such fine features are often washed out in less pure samples.

Inspired by the results of p-MBT, we further performed the nanocluster synthesis by utilizing m-MBT. Originally, we thought the same $Au_{130}(SR)_{50}$ magic size would be the final product after size-focusing, because m-MBT closely resembles p-MBT and the only noticeable change is the position of the methyl group. But surprisingly, we obtained a new 25 kDa species after the size focusing process (Figure 3a). We labeled the new cluster as M_m. The UV−vis spectrum of M_m showed absorption bands at ∼420, ∼630, and ∼720 nm (Figure 3b), which is clearly different from the spectrum of the above $Au_{130}(p\text{-MBT})_{50}$.

ESI-MS and TGA were conducted to determine the formula of the M_m nanocluster. In ESI-MS, two prominent peaks at m/z = 8600.44 and 12834.15 (along with a small peak at m/z = 17067.99) were observed (Figure 3c). The ratio between the two prominent peaks is 0.67, suggesting the first peak is 3+ charged and the second peak is 2+ charged. The assignment of the exact formula is somewhat less straightforward than the above $Au_{130}(p\text{-MBT})_{50}$ case. We first assume that the m/z 8600.44 peak corresponds to $[M_mCs_3]^{3+}$ and the m/z 12834.15 peak to $[M_mCs_2]^{2+}$. In that case, the molecular weight of M_m is 25402.54 (averaged over the 3+ and 2+ peaks after subtracting the cesium ions). Then we conducted TGA on the M_m nanocluster, and the result showed the weight loss to be 20.2%, that is, the Au/S molar ratio of 1/0.40 (Figure 3d). However, with the molecular weight of M_m being 25402.54 no formula satisfactorily matches with the experimental data (Supporting Information Table S2). Therefore, we suspect the possible charging effect of the gold core, which may occur in some cases during the ESI analysis;[39] here we reassign the 8600.44 and 12834.15 peaks as $[M_mCs_2]^{3+}$ and $[M_mCs]^{2+}$, respectively, in which one Cs ion is removed in both peaks and the metal core thus carries 1+ charge due to the ESI induction.
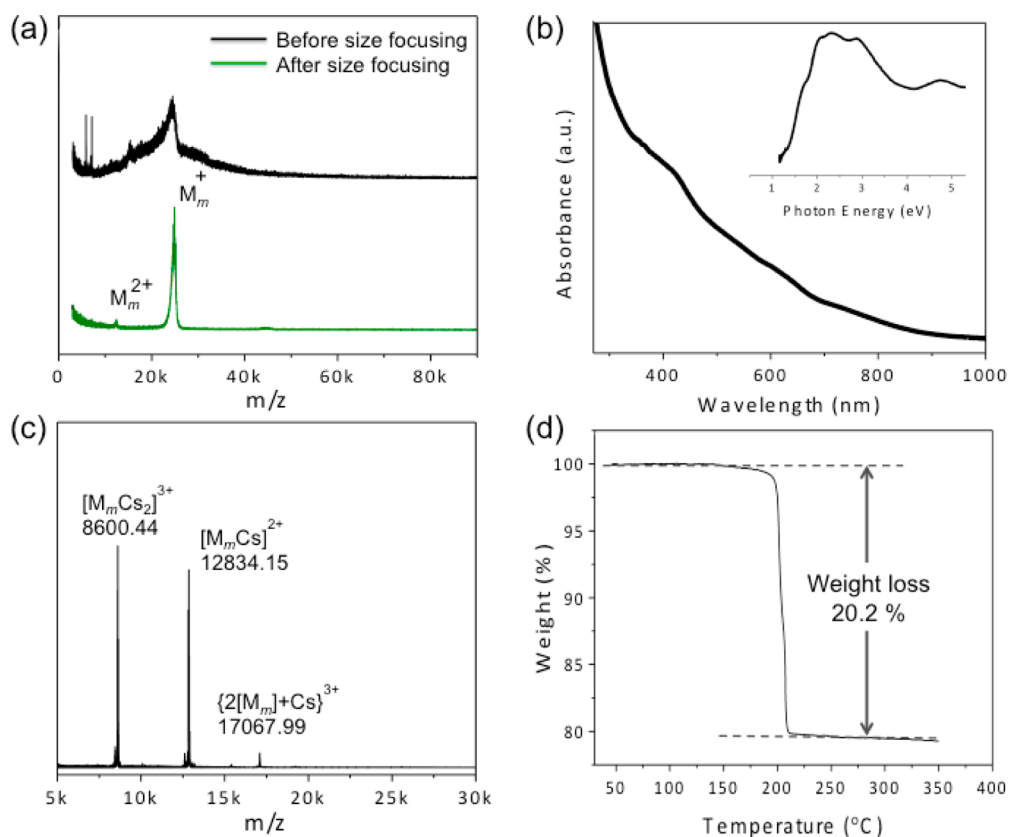
Figure 3. $Au_{104}(m\text{-MBT})_{41}$ nanocluster. (a) MALDI-MS spectra before/after size-focusing; (b) UV−vis spectrum, inset: photon-energy plot; (c) ESI-MS; (d) TGA.

On the basis of this, the average molecular weight is 25536.32. We then searched the possible combinations of the gold atom and thiolate ligand numbers for the M_m nanocluster (Supporting Information Table S3) and found that the formula of $Au_{104}(m\text{-MBT})_{41}$ satisfies both the experimental molecular weight of 25536.32 (theoretical, 25536.08; deviation −0.24) and the TGA data (theoretical, 19.8%; deviation −0.4%). On the basis of the $Au_{104}(m\text{-MBT})_{41}$ formula, the third peak in the ESI-MS (Figure 3c) is due to $\{2[Au_{104}(m\text{-MBT})_{41}]+Cs]\}^{3+}$ (theoretical, 17067.98; deviation −0.01). The $Au_{104}(m\text{-MBT})_{41}$ formula is further confirmed by the synthesis of phenyl-ethylthiolate-protected counterpart, which exhibits a mass difference of 575 Da and this mass difference when divided by the 14 Da mass difference of the two types of ligands gives rise to 41.07 (i.e., 41 ligands in both clusters, see Supporting Information Figure S5).

The $Au_{104}(m\text{-MBT})_{41}$ or $Au_{104}(SC_2H_4Ph)_{41}$ constitutes a new magic size of atomically precise gold nanoclusters. Of note, Dass et al.[43] previously reported a mixture containing $Au_{103}(SR)_{45}$, $Au_{104}(SR)_{45}$, $Au_{104}(SR)_{46}$, and $Au_{105}(SR)_{46}$ (R = C_2H_4Ph). Supporting Information Figure S3 compares the optical spectra of $Au_{104}(m\text{-MBT})_{41}$ and the size-mixed $Au_{103-105}(SR)_{45-46}$ sample. To further analyze the charge state of the $Au_{104}(m\text{-MBT})_{41}$ cluster (because ESI points to a 1+ charge state of the metal core), we carried out X-ray photoelectron spectroscopy (XPS) analysis on $Au_{104}(m\text{-MBT})_{41}$ (Supporting Information Figure S6) and ruled out the presence of Br⁻ or Cl⁻, which would be the possible counterion if the nanocluster were to carry an inherent positive charge. The other possibility (i.e., anionic $Au_{104}(m\text{-MBT})_{41}$) can also be ruled out, because if so, TOA⁺ would be the

counterion, but XPS analysis did not find the N(1s) signal (binding energy: 401.6 eV). These results indicate that the 1+ core charge observed in the adducts $[Au_{104}(m\text{-MBT})_{41}Cs]^{2+}$ and $[Au_{104}(m\text{-MBT})_{41}Cs_2]^{3+}$ in ESI-MS analysis was caused by in-source ionization process, as was the case of $Au_{144}(SR)_{60}$.[39] Thus, the $Au_{104}(m\text{-MBT})_{41}$ or $Au_{104}(SC_2H_4Ph)_{41}$ cluster is charge-neutral in the native state.

On the basis of the above results that p-MBT and m-MBT can result in different magic sizes during the size-focusing process under otherwise similar synthetic conditions, we further wonder whether the o-MBT, that is, by moving the methyl group closer to the sulfur atom, would produce any new magic size other than $Au_{130}(p\text{-MBT})_{50}$ and $Au_{104}(m\text{-MBT})_{41}$. This is indeed the case and we observed a smaller magic size: $Au_{40}(o\text{-MBT})_{24}$. The $Au_{40}(SR)_{24}$ formula was previously reported;[44,45] the phenylethylthiolate-capped $Au_{40}(SC_2H_4Ph)_{24}$ was found to be existent as an intermediate in the size-focusing process for synthesizing the $Au_{38}(SC_2H_4Ph)_{24}$ nanocluster.[44] In that case, $Au_{40}(SC_2H_4Ph)_{24}$ was somewhat less stable than $Au_{38}(SC_2H_4Ph)_{24}$ and thus was converted to $Au_{38}(SC_2H_4Ph)_{24}$ eventually. But if one terminates the size focusing reaction before Au_{40} was completely converted to Au_{38}, $Au_{40}(SC_2H_4Ph)_{24}$ can be isolated by size exclusion chromatography.[44] In the present work, we observed that when o-MBT was used, the final size-focusing product was surprisingly $Au_{40}(o\text{-MBT})_{24}$ instead of $Au_{38}(o\text{-MBT})_{24}$ (Figure 4a and Supporting Information Figure S7). We note that the $Au_{40}(o\text{-MBT})_{24}$ nanocluster obtained in the present work is highly robust under the size focusing conditions (i.e., no conversion to $Au_{38}(o\text{-MBT})_{24}$ even after a prolonged reaction); thus, the
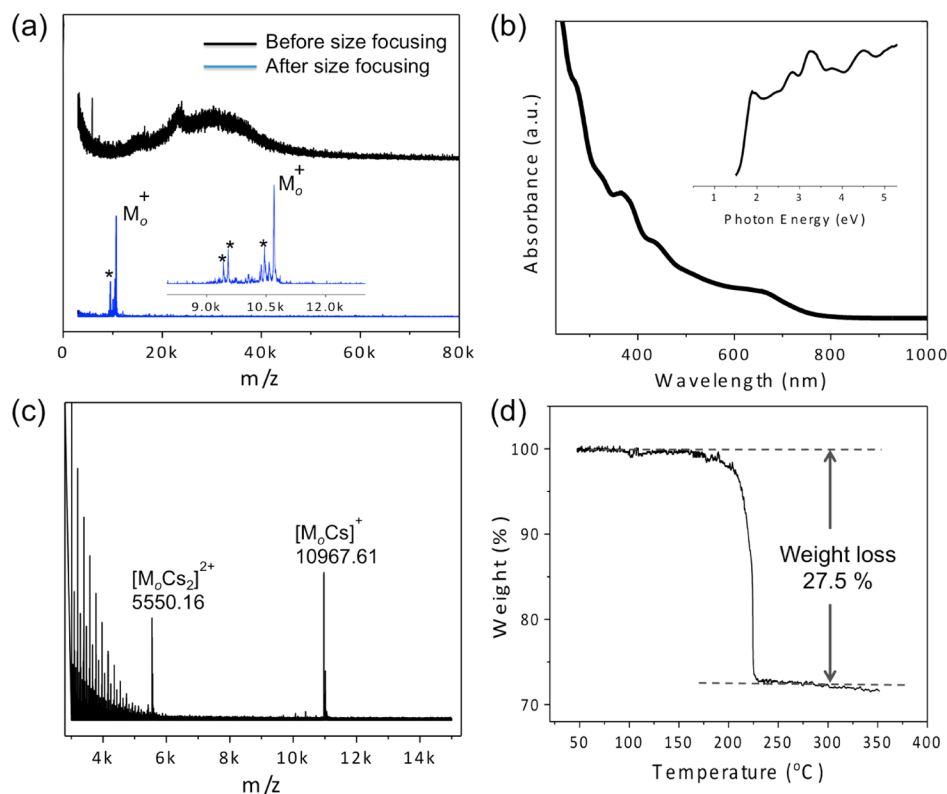
Figure 4. $Au_{40}(o\text{-MBT})_{24}$ nanocluster. (a) MALDI-MS spectra before/after size-focusing. The asterisks indicate the fragments; (b) UV−vis spectrum, inset: photon-energy plot; (c) ESI-MS, the lower m/z comb-like peaks are caused by $(CsOAc)_n Cs^+$; (d) TGA.

present $Au_{40}(o\text{-MBT})_{24}$ is probably a different isomer than the previously reported $Au_{40}(SC_2H_4Ph)_{24}$ nanocluster.

The absorption spectrum of $Au_{40}(o\text{-MBT})_{24}$ showed two distinct peaks at ∼365 and ∼430 nm along with a relatively flat band at ∼657 nm (Figure 4b). The formula of $Au_{40}(o\text{-MBT})_{24}$ (denoted as M_o) is unambiguously determined by ESI-MS in conjunction with TGA (Figure 4c,d). Briefly, the molecular weight (MW) for the M_o nanocluster is determined to be 10834.62 based on the doubly charged $[M_o Cs_2]^{2+}$ (5550.16, that is, MW = 10834.52) and singly charged $[M_o Cs]^+$ (10967.61, that is, MW = 10834.71) in ESI-MS (Figure 4c, and Supporting Information Figure S1e,f for zoom-in 1+ and 2+ peaks). The weight loss in TGA analysis of this cluster is 27.5%, corresponding to Au/SR molar ratio of 1/0.61. The theoretical molecular weight of $Au_{40}(o\text{-MBT})_{24}$ is 10834.86 (deviation, 0.24) and theoretical weight loss is 27.3% (deviation, −0.2%). Other possible formulas all deviate significantly from the ESI data (Supporting Information Table S4). The optical spectra of the previously reported $Au_{40}(SR)_{24}$ nanoclusters[44,45] show large differences from that of the present $Au_{40}(o\text{-MBT})_{24}$ (Supporting Information Figure S4) due to the isomer formation.

The above results explicitly demonstrate that by subtle adjusting of the structure of the surface-protecting thiolate ligand, three different magic sizes (i.e., $Au_{130}(p\text{-MBT})_{50}$, $Au_{104}(m\text{-MBT})_{41}$, and $Au_{40}(o\text{-MBT})_{24}$) are exclusively synthesized with true monodispersity. In order to gain more insights into this intriguing phenomenon, we further performed time-dependent MALDI-MS to monitor the reaction progress. Supporting Information Figure S8 showed the detailed size-focusing process of $Au_{130}(p\text{-MBT})_{50}$. It is found that during the reaction process, Au_{130} and a ∼24 kDa species were formed

after 5 h of size-focusing (Supporting Information Figure S8, red profile). However, the abundance of the 24 kDa species gradually decreases relative to Au_{130} as the reaction proceeds, implying that the 24 kDa species is only metastable (less stable than Au_{130}) under the p-MBT size focusing conditions. For the case of m-MBT, there are also two sizes observed during size-focusing, that is, $Au_{104}(m\text{-MBT})_{41}$ and a metastable ∼30 kDa species (Supporting Information Figure S9); the 30 kDa size phases out under the m-MBT conditions. For the case of o-MBT, the initial products over the course of size-focusing include a ∼24 kDa species, $Au_{40}(o\text{-MBT})_{24}$ and $Au_{38}(o\text{-MBT})_{24}$ (Supporting Information Figure S10); among them, the ∼24 kDa species first disappeared as the reaction proceeded, then the Au_{38} nanoclusters, and finally pure Au_{40} nanoclusters were resulted. On the basis of the time-dependent analysis of reaction intermediates, we can conclude that the selective syntheses of $Au_{130}(p\text{-MBT})_{50}$, $Au_{104}(m\text{-MBT})_{41}$, and $Au_{40}(o\text{-MBT})_{24}$ are due to the preferential stabilization of different magic sizes by the different MBT isomers under the size-focusing conditions.

While distinctly different ligands are well-known to lead to different sizes of nanoclusters as demonstrated in previous cases of thiolate and phosphine ligands,[30,46] our discovery that the subtle ligand structural difference (i.e., the position of methyl group in MBT thiol) can lead to different cluster sizes (i.e., Au_{130}, Au_{104} and Au_{40}) under otherwise similar synthetic conditions is indeed remarkable and unexpected. An interesting question is why the subtle difference of the protecting thiol structure can give rise to such drastic impacts on the resulting magic sizes. As demonstrated in this work, when changing the methyl group from the para- to meta- and to ortho-position, the most stable size changes from $Au_{130}(p\text{-MBT})_{50}$ to $Au_{104}(m\text{-}$

MBT)$_{41}$ then to Au$_{40}$(o-MBT)$_{24}$. The shrinkage of the magic sizes may be attributed to the difference in the steric hindrance among the three isomeric methylbenzenethiols: the closer the methyl group to the sulfur atom in the thiol, the more structural hindrance would occur in the gold–sulfur interface. Thus, the o-MBT in which the methyl group is closest to the sulfur atom tends to stabilize the smallest Au$_{40}$ nanocluster among the three magic sizes. On the other hand, the methyl group in the p-MBT is farthest from the sulfur atom, corresponding to the least perturbation to the Au–S interfacial bond and thus gives rise to the largest Au$_{130}$ nanocluster among the series. Therefore, the o-, m-, and p-MBT ligands lead to different strain on the Au–S interfacial bond, which affects the size of the cluster. Overall, the stability of magic size nanoclusters is a combined result of both the surface protecting ligand and the core structure. Of note, the Au$_{130}$(p-MBT)$_{50}$, Au$_{104}$(m-MBT)$_{41}$, and Au$_{40}$(o-MBT)$_{24}$ are stable for at least six months (note: long times have not been investigated). We further point out that the size and structure of gold nanoclusters become sensitive to the subtle structural change of protecting thiols only when the thiolate ligand's backbone is rigid such as the MBT cases; if the thiolate ligand's backbone is flexible, the structure of thiolate ligands does not show a dramatic impact on the resulting sizes of nanoclusters. This explains why phenylethylthiol (PhC$_2$H$_4$SH), aliphatic thiols (C$_n$H$_{2n+1}$SH), and glutathione (GSH) show similar magic sizes, despite their different structures or bulkiness. For example, the Au$_{25}$(SR)$_{18}$ nanocluster has a high tolerance to ligand structure,[1,2,4,37] but it converts to Au$_{20}$(SPh-^{t}Bu)$_{16}$ when reacting with excess HSPh-^{t}Bu under thermal conditions.[5]

In summary, we have revealed that the magic sizes of gold nanoclusters are sensitive to the subtle structural change of the surface protecting ligands with rigid backbones. The isomeric methylbenzenethiols (p, m, and o-isomers) are used to demonstrate this strategic concept, and size-selective syntheses of Au$_{130}$(p-MBT)$_{50}$, Au$_{104}$(m-MBT)$_{41}$, and Au$_{40}$(o-MBT)$_{24}$ are attained. The Au–S interfacial bond stress is rationalized to be responsible for the observed trend of decreasing size (i.e., from Au$_{130}$ to Au$_{104}$ to Au$_{40}$) with increasing Au–S bond stress when going from the p-MBT to m-MBT to o-MBT ligand. The results of the present study shed light on the intriguing role of surface protecting thiols in dictating the magic size and stability of gold nanoclusters, which may permit the development of systematic synthetic approaches for the discovery of new magic-sized gold nanoclusters in future efforts.

■ ASSOCIATED CONTENT

Ⓢ Supporting Information

Details of the syntheses, characterizations, supporting Figures S1–10, and Tables S1–4. This material is available free of charge via the Internet at http://pubs.acs.org.

■ AUTHOR INFORMATION

Corresponding Author

*E-mail: rongchao@andrew.cmu.edu.

Notes

The authors declare no competing financial interest.

■ ACKNOWLEDGMENTS

■ REFERENCES

(1) Qian, H.; Zhu, M.; Wu, Z.; Jin, R. Acc. Chem. Res. 2012, 45, 1470−1479.
(2) Maity, P.; Xie, S.; Yamauchi, M.; Tsukuda, T. Nanoscale 2012, 4, 4027−4037.
(3) Price, R. C.; Whetten, R. L. J. Am. Chem. Soc. 2005, 127, 13750−13751.
(4) Parker, J. F.; Fields-Zinna, C. A.; Murray, R. W. Acc. Chem. Res. 2010, 43, 1289−1296.
(5) Zeng, C.; Liu, C.; Chen, Y.; Rosi, N. L.; Jin, R. J. Am. Chem. Soc. 2014, 136, 11922−11925.
(6) Wan, X.-K.; Lin, Z.-W.; Wang, Q.-M. J. Am. Chem. Soc. 2012, 134, 14750−14752.
(7) Yang, H.; Wang, Y.; Yan, J.; Chen, X.; Zhang, X.; Häkkinen, H.; Zheng, N. J. Am. Chem. Soc. 2014, 136, 7197−7200.
(8) Zeng, C.; Chen, Y.; Li, G.; Jin, R. Chem. Commun. 2014, 50, 55−57.
(9) Hudgens, J. W.; Pettibone, J. M.; Senftle, T. P.; Bratton, R. N. Inorg. Chem. 2011, 50, 10178−10189.
(10) Song, Y.; Wang, S.; Zhang, J.; Kang, X.; Chen, S.; Li, P.; Sheng, H.; Zhu, M. J. Am. Chem. Soc. 2014, 136, 2963−2965.
(11) Tang, Q.; Jiang, D.-e. J. Phys. Chem. C 2014, DOI: 10.1021/jp508883v.
(12) Knoppe, S.; Wong, O. A.; Malola, S.; Häkkinen, H.; Bürgi, T.; Verbiest, T.; Ackerson, C. J. J. Am. Chem. Soc. 2014, 136, 4129−4132.
(13) Kauffman, D. R.; Alfonso, D.; Matranga, C.; Qian, H.; Jin, R. J. Am. Chem. Soc. 2012, 134, 10237−10243.
(14) Xie, S.; Tsunoyama, H.; Kurashige, W.; Negishi, Y.; Tsukuda, T. ACS Catal. 2012, 2, 1519−1523.
(15) Li, G.; Jiang, D.-e.; Kumar, S.; Chen, Y.; Jin, R. ACS Catal. 2014, 4, 2463−2469.
(16) Chen, Y.-S.; Choi, H.; Kamat, P. V. J. Am. Chem. Soc. 2013, 135, 8822−8825.
(17) Chevrier, D. M.; Chatt, A.; Zhang, P.; Zeng, C.; Jin, R. J. Phys. Chem. Lett. 2013, 36, 3186−3191.
(18) Luo, Z.; Yuan, X.; Yu, Y.; Zhang, Q.; Leong, D. T.; Lee, J. Y.; Xie, J. J. Am. Chem. Soc. 2012, 134, 16662−16670.
(19) Zheng, J.; Zhou, C.; Yu, M.; Liu, J. Nanoscale 2012, 4, 4073−4083.
(20) Li, G.; Zeng, C.; Jin, R. J. Am. Chem. Soc. 2014, 136, 3673−3679.
(21) Ghosh, A.; Udayabhaskararao, T.; Pradeep, T. J. Phys. Chem. Lett. 2012, 3, 1997−2002.
(22) Kawasaki, H.; Kumar, S.; Li, G.; Zeng, C.; Kauffman, D. R.; Yoshimoto, J.; Iwasaki, Y.; Jin, R. Chem. Mater. 2014, 26, 2777−2788.
(23) Jin, R. Nanoscale 2015, 7, 1549−1565.
(24) Negishi, Y.; Nobusada, K.; Tsukuda, T. J. Am. Chem. Soc. 2005, 127, 5261−5270.
(25) Zeng, C.; Chen, Y.; Li, G.; Jin, R. Chem. Mater. 2014, 26, 2635−2641.
(26) Levi-Kalisman, Y.; Jadzinsky, P. D.; Kalisman, N.; Tsunoyama, H.; Tsukuda, T.; Bushnell, D. A.; Kornberg, R. D. J. Am. Chem. Soc. 2011, 133, 2976−2982.
(27) Jiang, D.-e. Nanoscale 2013, 5, 7149−7160.
(28) Jin, R.; Qian, H.; Wu, Z.; Zhu, Y.; Zhu, M.; Mohanty, A.; Garg, N. J. Phys. Chem. Lett. 2010, 1, 2903−2910.
(29) Qian, H.; Zhu, Y.; Jin, R. ACS Nano 2009, 3, 3795−3803.
(30) Krommenhoek, P. J.; Wang, J.; Hentz, N.; Johnston-Peck, A. C.; Kozek, K. A.; Kalyuzhny, G.; Tracy, J. B. ACS Nano 2012, 6, 4903−4911.
(31) Nishigaki, J.-i.; Tsunoyama, R.; Tsunoyama, H.; Ichikuni, N.; Yamazoe, S.; Negishi, Y.; Ito, M.; Matsuo, T.; Tamao, K.; Tsukuda, T. J. Am. Chem. Soc. 2012, 134, 14295−14297.
(32) Zeng, C.; Qian, H.; Li, T.; Li, G.; Rosi, N. L.; Yoon, B.; Barnett, R. N.; Whetten, R. L.; Landman, U.; Jin, R. Angew. Chem., Int. Ed. 2012, 51, 13114−13118.
(33) Zeng, C.; Liu, C.; Pei, Y.; Jin, R. ACS Nano 2013, 7, 6138−6145.

(34) Nishigaki, J.-i.; Yamazoe, S.; Kohara, S.; Fujiwara, A.; Kurashige, W.; Negishi, Y.; Tsukuda, T. *Chem. Commun.* **2014**, *50*, 839−841.

(35) Shichibu, Y.; Negishi, Y.; Tsukuda, T.; Teranishi, T. *J. Am. Chem. Soc.* **2005**, *127*, 13464−13465.

(36) Zhu, M.; Lanni, E.; Garg, N.; Bier, M. E.; Jin, R. *J. Am. Chem. Soc.* **2008**, *130*, 1138−1139.

(37) De Nardi, M.; Antonello, S.; Jiang, D.-e.; Pan, F.; Rissanen, K.; Ruzzi, M.; Venzo, A.; Zoleo, A.; Maran, F. *ACS Nano* **2014**, *8*, 8505−8512.

(38) Chaki, N. K.; Negishi, Y.; Tsunoyama, H.; Shichibu, Y.; Tsukuda, T. *J. Am. Chem. Soc.* **2008**, *130*, 8608−8610.

(39) Qian, H.; Jin, R. *Nano Lett.* **2009**, *9*, 4083−4087.

(40) Negishi, Y.; Sakamoto, C.; Ohyama, T.; Tsukuda, T. *J. Phys. Chem. Lett.* **2012**, *3*, 1624−1628.

(41) Tang, Z.; Robinson, D. A.; Bokossa, N.; Xu, B.; Wang, S.; Wang, G. *J. Am. Chem. Soc.* **2011**, *133*, 16037−16044.

(42) Jupally, V. R.; Dass, A. *Phys. Chem. Chem. Phys.* **2014**, *16*, 10473−10479.

(43) Dass, A.; Nimmala, P. R.; Jupally, V. R.; Kothalawala, N. *Nanoscale* **2013**, *5*, 12082−12085.

(44) Qian, H.; Zhu, Y.; Jin, R. *J. Am. Chem. Soc.* **2010**, *132*, 4583−4585.

(45) Knoppe, S.; Boudon, J.; Dolamic, I.; Dass, A.; Bürgi, T. *Anal. Chem.* **2011**, *83*, 5056−5061.

(46) Mingos, D. M. P. *Inorg. Chem.* **1982**, *21*, 464−466.